International Journal of Biological Macromolecules 250 (2023) 126164

Contents lists available at ScienceDirect

International Journal of Biological Macromolecules

journal homepage: www.elsevier.com/locate/ijbiomac

Protein features instruct the secretion dynamics from metal-supported synthetic amyloids

Eloi Parladé [a,b,c,*], Julieta M. Sánchez [a,b,c,d,e], Hèctor López-Laguna [a,b], Ugutz Unzueta [a,c,f,g], Antonio Villaverde [a,b,c], Esther Vázquez [a,b,c,*]

[a] CIBER de Bioingeniería, Biomateriales y Nanomedicina (CIBER-BBN, ISCIII), Universitat Autònoma de Barcelona, 08193 Bellaterra, Spain
[b] Institut de Biotecnologia i de Biomedicina, Universitat Autònoma de Barcelona, 08193 Bellaterra, Spain
[c] Departament de Genètica i de Microbiologia, Universitat Autònoma de Barcelona, 08193 Bellaterra, Spain
[d] Departamento de Química, Cátedra de Química Biológica, Facultad de Ciencias Exactas, Físicas y Naturales, ICTA, Universidad Nacional de Córdoba, Av. Vélez Sársfield 1611, Córdoba 5016, Argentina
[e] Instituto de Investigaciones Biológicas y Tecnológicas (IIByT), CONICET-Universidad Nacional de Córdoba, Córdoba 5016, Argentina
[f] Institut d'Investigació Biomèdica Sant Pau (IIB SANT PAU), Sant Quintí 77-79, 08041 Barcelona, Spain
[g] Josep Carreras Leukaemia Research Institute, 08025 Barcelona, Spain

ARTICLE INFO

Keywords:
Recombinant proteins
Microparticles
Secretory amyloids
Drug delivery system
Time sustained drug release
Building blocks

ABSTRACT

Hexahistidine-tagged proteins can be clustered by divalent cations into self-containing, dynamic protein depots at the microscale, which under physiological conditions leak functional protein. While such protein granules show promise in clinics as time-sustained drug delivery systems, little is known about how the nature of their components, that is, the protein and the particular cation used as cross-linker, impact on the disintegration of the material and on its secretory performance. By using four model proteins and four different cation formulations to control aggregation, we have here determined a moderate influence of the used cation and a potent impact of some protein properties on the release kinetics and on the final fraction of releasable protein. In particular, the electrostatic charge at the amino terminus and the instability and hydropathicity indexes determine the disintegration profile of the depot. These data offer clues for the fabrication of efficient and fully exploitable secretory granules that being biocompatible and chemically homogenous allow their tailored use as drug delivery platforms in biological systems.

1. Introduction

Artificial systems for the slow leakage of functional proteins show promise as sustained drug delivery systems [1,2]. Among them, microscale clusters of hexahistidine (H6)-tagged proteins are fabricated using divalent cations, that such as Zn^{2+}, crosslink polypeptide chains through solvent-exposed histidine residues, in a reversible way [3–5]. Therefore, in contrast to other protein release platforms based on holding matrices, self-contained secretory granules fabricated in vitro disintegrate, in biological interfaces, into their building block polypeptides that act as drug and mechanically stable scaffold at the same time [6]. The use of this platform as a drug delivery system is feasible since the released polypeptides are properly folded and fully functional, enabling complex activities such as tumor targeting [7] or promotion of cell proliferation [8]. Such self-delivery of the forming protein molecules occurs by a process that might involve the loss of gluing cations, either by chelation or physiological dilution, what allows a progressive disintegration of the material and the resulting secretion event [9–11]. The self-containing nature of such protein depots, the amyloidal architecture and the involvement of divalent cations as cross-linking agents are properties similar to those found in functional amyloids occurring in nature [12–16], such as secretory granules in the human endocrine system [10,11,17,18] and bacterial inclusion bodies [19]. Also, the absence of any potentially toxic, non-protein sponge-like material acting as drug container or bulk material, not only simplifies the fabrication process but also alleviates safety concerns [20]. In this regard, the generation of the microscale granules is based on one single mixing (protein and cation) step [21] what allows envisaging industrial-scale production. Furthermore, the lack of heterologous holder materials also precludes any trace of toxicity linked to the delivery system and makes the whole

* Corresponding authors at: Universitat Autònoma de Barcelona, Edifici MRB. Carrer de la Vinya, s/n. Campus, 08193 Cerdanyola del Vallès, Barcelona, Spain.
E-mail addresses: eloi.parlade@uab.cat (E. Parladé), esther.vazquez@uab.cat (E. Vázquez).

https://doi.org/10.1016/j.ijbiomac.2023.126164
Received 16 May 2023; Received in revised form 3 August 2023; Accepted 4 August 2023
Available online 6 August 2023

concept robust enough for regulatory demands and clinical adaptation. Importantly, the building blocks for the fabrication of secretory granules can be either plain polypeptides or protein oligomers, that in both cases keep their biological activity once released from the depots, in vitro and in vivo [22,23].

A main issue to be solved in the clinically oriented development of these systems is how to approach the regulation of the release dynamics of the embedded protein, or instead, which protein or fabrication features might determine, as a whole, the secretory properties of such depots. Being artificial secretory amyloids an emerging, still poorly explored platform, we have screened here this category of materials as formed by several recombinant proteins and divalent cations. By doing that, key physicochemical properties of the building block protein have been identified that define the performance and release kinetics from the granular depots during their physiological disintegration. This insight opens a door to a tailored fabrication of secretory microscale granules aiming at particular secretory profiles.

2. Experimental section

2.1. Protein production and characterization

Four proteins, namely GFP-H6, T22-GFP-H6, EPIXRK-GFP-H6 and T22-HSNBT-H6, had been designed in house and the respective encoding genes provided by GeneArt (Thermo Fisher, Waltham, MA, USA), as subcloned into the plasmid pET22b (Merck, Darmstadt, Germany). T22 [24] and EPIXRK [25] are cationic peptides selectively binding the tumoral marker CXCR4. HSNBT is a modified domain of the human nidogen with structural similarities to GFP [26]. Both proteins have been used as scaffold materials for tumor-targeted, drug carrying nanoparticles. Plasmids encoding the proteins were transformed into *Escherichia coli* Origami B (DE3). Proteins were produced overnight at 20 °C in Lysogeny Broth (LB) medium upon induction with 0.1 mM isopropyl-β-D-1-tiogalactopyranoside. Then, cells were harvested by centrifugation at 5000*g* for 15 min and resuspended in wash buffer (20 mM Tris, 500 mM NaCl, 10 mM Imidazole, pH 8) in the presence of protease inhibitor (cOmplete™ EDTA-Free, Roche, Basel, Switzerland). Cell lysis was achieved by subjecting the protein to high pressure for three rounds at 8000 psi in an EmulsiFlex-C5 system (Avestin, Ottawa, ON, Canada). The soluble fractions of cell lysates containing each protein of interest were separated by centrifugation at 15,000*g* during 45 min and then charged into HisTrap HP columns (Cytiva, Marlborough, MA, USA) for purification by immobilized metal affinity chromatography (IMAC) in an ÄKTA pure system (Cytiva, Marlborough, MA, USA). Protein elution was attained by applying a linear gradient of elution buffer (20 mM Tris, 500 mM NaCl, 500 mM Imidazole, pH 8). Purified protein fractions were then dialyzed and stored in sodium carbonate (166 mM $NaCO_3H$, pH 8), or saline sodium carbonate (166 mM $NaCO_3H$, 333 mM NaCl, pH 8), in the case of T22-GFP-H6. Protein purity and molecular mass were verified by SDS-PAGE gel electrophoresis and subsequent Western blot immunodetection using an anti-His monoclonal antibody (Santa Cruz Biotechnology, Dallas, TX, USA) (Supplementary Fig. 1). Protein concentration was always determined via Bradford assay (Bio-Rad, Hercules, CA, USA).

2.2. Fabrication of secretory granules

To produce the secretory granules, 100 μg of each pure soluble protein were precipitated with an excess of four different divalent cation salt combinations, namely $ZnCl_2$, $CaCl_2$, $MnCl_2$ and $ZnCl_2$ + $CaCl_2$. Precipitation reactions were carried out in phosphate-buffered saline (PBS) at physiological pH 7.4 in a final volume of 100 μl and final protein concentration of 1 mg/ml. After mixing the protein with the divalent ions in Eppendorf tubes, reactions were gently homogenized and left to react for 10 min, after which centrifugation at 15,000*g* for 15 min was used to separate the microgranules in the insoluble fraction from the unreacted soluble protein in the supernatant. Molar excess ratios of divalent cations were defined as 1:300, 1:2000, 1:1200 and 1:150 + 1500 (protein:cation) for Zn, Ca, Mn and Zn + Ca, respectively, based on previous studies [27]. The efficiency of precipitation for each protein and divalent cation combination was studied by comparing the soluble protein remaining in every reaction supernatant with the soluble protein in the supernatant of a control reaction, performed in PBS, without any divalent cation salt.

2.3. Assay of granule disintegration and protein release

A protein release assay was designed in which microgranules formed from 100 μg of each soluble protein were incubated for 21 days at 37 °C in PBS (pH 7.4). The released soluble protein was fully harvested from the supernatant at days 1, 2, 3, 7, 14 and 21 by centrifugation at 15,000*g* for 10 min, and fresh PBS was added to replace the subtracted volume. By the end of the 21 incubation days, the insoluble material was exposed to EDTA at the same molar concentration that the divalent cation used for the precipitation of each respective protein, to recover the total amount of chelated protein available in the granules. Finally, materials based on several protein-ion combinations were exposed to 5 mM dithiothreitol (DTT) and 10 mM EDTA to test whether disulfide bonds were responsible for the protein remaining in granular form even after chelation. To visualize the cumulative release of proteins from the granules over the course of the experiment, the plots were generated using the accumulated data for each day.

2.4. Morphometric and physicochemical characterization of protein materials

The protein hydrodynamic diameter was determined by Dynamic Light Scattering (DLS) at 633 nm and 25 °C in a Zetasizer Nano ZS (Malvern Instruments, Malvern, United Kingdom), using low volume cuvettes. All particle measurements were performed in triplicate. Only the most abundant peak (as measured by percent volume) in each measurement was used to calculate average peak sizes. Images of the precipitated granules were acquired in a ZEISS Merlin® FESEM (ZEISS, Oberkochen, Germany). Electron high tension was set at 2 kV and signal was taken using the secondary electron detector. Protein fluorescence was measured in a Qubit 4 fluorometer (Invitrogen, Waltham, MA, USA) by excitation at 470 nm (blue) and detection at the 510–580 nm range (green). Theoretical physicochemical properties (i.e. Aliphatic index, GRAVY, Instability index), were calculated from the amino acid sequences via the ProtParam tool on the Expasy Server [28]. Theoretical absolute charge for each protein at pH 7.4 was calculated using the Peptides R package in the Lehninger pK scale (R version 4.2.1) [29].

2.5. Determination of amyloid content

Amyloid content in T22-HSNBT-H6 protein granules was determined using the Thioflavin T (ThT) assay. Briefly, 25 μM of ThT (Sigma-Aldrich) was added to 0.1 mg/ml of the protein sample in PBS. Fluorescence intensity was registered at 485 nm after excitation at 450 nm in a Varian Cary Eclipse spectrofluorometer (Agilent Technologies, Santa Clara, CA, USA). The cross-beta-sheet structure of the protein cluster was distinguished from the control soluble protein by the increase in dye fluorescence emission caused by the interaction with amyloidogenic protein. GFP-containing constructs could not be assessed via the ThT assay due to the interference of their inherent fluorescence emission. In such cases, amyloid content was measured using attenuated total reflectance-Fourier transform infrared spectroscopy (ATR-FTIR). In this method, insoluble protein samples were placed in a Tensor 27 Bruker spectrometer with a Specac's Golden Gate Attenuated Total Reflectance (ATR) accessory. Measurements were done at room temperature in a continuous N_2 flow, on spectroscopic crystal surfaces. Spectra were recorded 16 times at a scan rate of 50 cm^{-1}/min with a nominal

resolution of 2 cm^{-1}. The absorbance values were corrected by subtracting the background. Fourier deconvolution of the spectra and the second derivative allowed the identification and analyses of different band components. The fitting of components to the original spectrum (prior to deconvolution) was performed assuming a Gaussian shape. All data were processed using Peakfit 4.1.2.

2.6. Statistical analyses and data plotting

Ordinary one-way ANOVA with post-hoc Tukey's test was used to evaluate differences in protein precipitation. A saturation model (Supplementary Eq. 1) was employed to fit the protein release data and extract relevant indexes using a confidence interval of 95 % and R squared was used to quantify the goodness-of-fit. All statistical analyses were performed in GraphPad Prism 8.0.2. All assays were performed at least in triplicate. Nested circle graphs were made using Matplotlib in Python 3.8.16 and the correlation matrix was plotted using the corrplot package in R 4.2.1. All other graphs were plotted in GraphPad Prism 8.0.2.

3. Results

Four H6-tagged proteins, which share specific domains (Fig. 1A, Supplementary Table 1) but with distinguishable physicochemical properties (Fig. 1B, Supplementary Table 2), were produced in recombinant *E. coli* and selected for pairwise comparison upon the construction of artificial secretory granules. In three of them, a cationic peptide (CP) was present at the amino-terminus of the construct (Fig. 1A). We were interested in determining which protein properties might be involved in the dynamic performance of the resulting depot material, that releases the building block protein in a time sustained way. The ability of the model polypeptides to precipitate into insoluble aggregates was tested by using four different formulations, which involved cationic forms of Ca, Mn and Zn. As observed (Fig. 1C, D), Ca was less capable, in comparison to alternative cations, to aggregate the soluble protein versions into insoluble material. In contrast, the Zn-based clustering was generically the most efficient. At exception of GFP-H6, the aggregation profile of the model proteins was very similar (Fig. 1C). However, the presence of a cationic peptide at the amino terminus was found as enhancer of aggregation, marginally when using Ca, but especially in Mn and Zn + Ca mixtures for protein clustering (Fig. 1D). The discrete, granular nature of the resulting protein aggregates was confirmed by Field-Emission Scanning Electron Microscopy (FESEM), that revealed the occurrence of particles sized between 2 and 15 μm in diameter (Fig. 1E, F). To assess that these structures were not mere metal precipitates, control FESEM images of mixtures of PBS and cation salts (in absence of protein) were taken (Supplementary Fig. 2). They showed precipitates larger and clearly distinct in their appearance and structure from those shown in Fig. 1E, F. This observation confirmed that as expected, the materials studied here were not artifacts formed by insoluble metal phosphates but true protein granules.

The aggregates formed through the above protocols, once washed, were incubated in physiological buffer at 37 °C, for increasing time periods and with replacement of the media. Such replacement was implemented to break any possible balance between insoluble and soluble agents that might inhibit any release, and to mimic, as much as possible, the waving in vivo conditions. The potential content of protein in the supernatant was periodically determined to assess the dynamic nature of the depots and to comparatively plot the kinetics of its release from the insoluble material. While EPIXRK-GFP-H6 was continuously leaked for at least 21 days from Ca-based granules, most of the proteins in most of the conditions showed an asymptotic release, with good fittings, which declined or stopped at around 7 days (Fig. 2A). Although some consistencies were found, such as the fact that Zn + Ca generically rendered materials with low protein leakage, a very divergent set of profiles was observed when comparing different proteins (Fig. 2A, B). This fact revealed an influence of the intrinsic protein properties on the capability of a particular protein to be released from the cation-

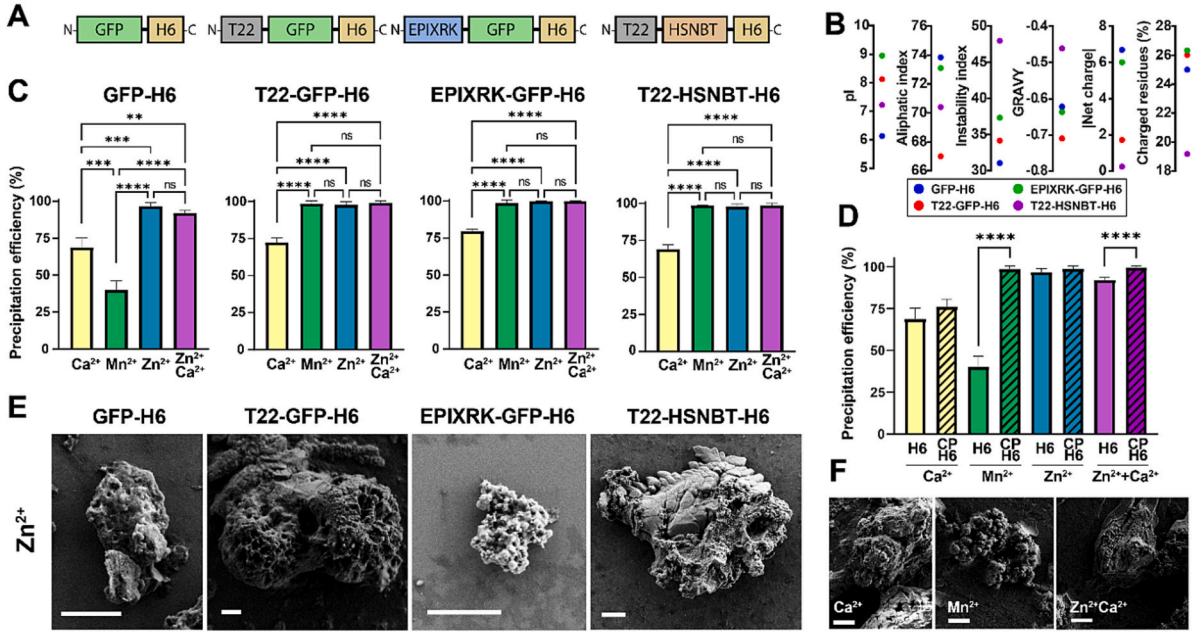

Fig. 1. A. Modular representation of the four protein models. Same colors indicate shared domains. B. Graphical representation of selected physicochemical parameters from Expasy's ProtParam. Values were calculated from the amino acid sequence of the chosen models. C. Percentage of soluble protein successfully precipitated after the addition of divalent cation salts of Ca, Mn, Zn and Zn + Ca, for each model protein. D. Percentage of soluble protein successfully precipitated after the addition of divalent cation salts to GFP-based proteins displaying only the His tag (H6) or displaying both a cationic N-terminal peptide and the His tag (CPH6, dashed bars). Statistical significance is represented as ** ($p < 0.01$), *** ($p < 0.001$), **** ($p < 0.0001$) and ns (not significant). E. Representative FESEM images of Zn-based secretory granules of each model protein. Scale bar: 2 μm. F. FESEM images of Ca, Mn and ZnCa-based secretory granules using the same model protein T22-GFP-H6. Scale bar: 2 μm.

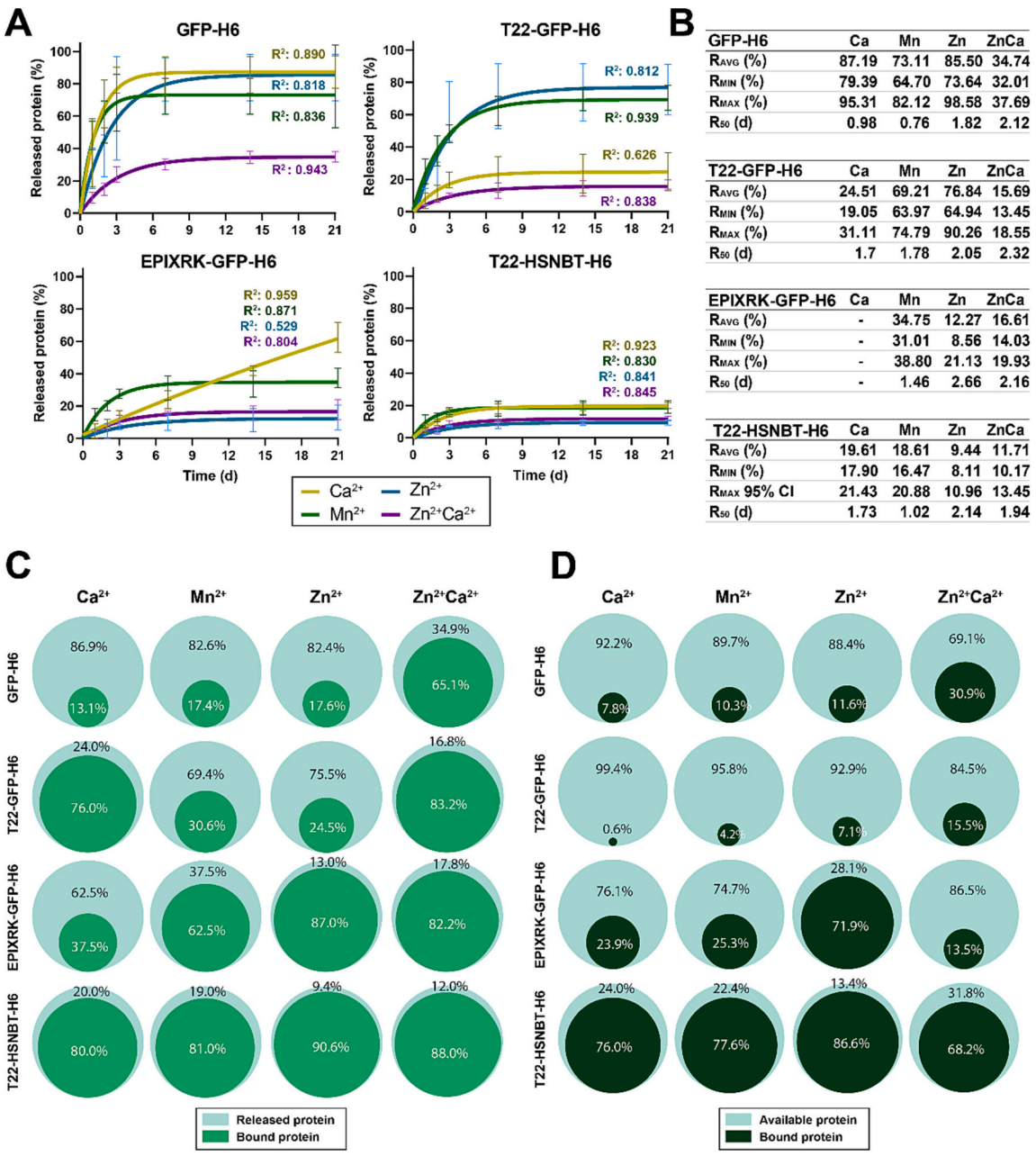

Fig. 2. A. Graphical representation of the soluble protein released from the secretory granules at different time points along a 21-day incubation. Each subsequent data point represents the newly solubilized protein added to the previous value. Data were fitted in a non-linear saturation model (Supplementary Eq. 1). B. Detailed information from each release curve indicating the average total of released protein (R_{AVG}), minimum (R_{MIN}) and maximum (R_{MAX}) release values in a 95 % confidence interval, and time at which half of the releasable protein has been liberated (R_{50}). C. Proportion of protein released at the endpoint (21 days) of the release assay (panel A) for each model and divalent cation combination tested. D. Proportion of protein available for release (sum of released protein after 21 days and EDTA-triggered release at the endpoint) for each model and divalent cation combination tested.

mediated clusters along time.

The protein released from each protein-ion combination granules was investigated using DLS to assess its size and implications following release (Supplementary Fig. 3A). Specifically, T22-GFP-H6 leaked from Zn-bound granules was chosen as the model protein for an in-depth study. Such analysis revealed a significantly larger size and the presence of multiple populations compared to nanoparticles formed by the same pure protein straightforwardly assembled with $ZnCl_2$ 0.04 mM (Supplementary Fig. 3B, green profiles). This observation suggested that Zn dragged from the granules and associated to the protein might be responsible for the observed high size. To verify this hypothesis, we conducted an additional experiment where EDTA was added to both T22-GFP-H6 control nanoparticles and the sub-micron particles released from the granules. The results demonstrated that both sample populations reverted their size to that of the soluble full-length protein form observed before any incubation (Supplementary Fig. 3B, black profiles). This observation further supports the role of bound Zn in enhancing the size of the released protein that is organized as oligomers. In addition to size analysis, we assessed the folding status of the solubilized T22-GFP-H6. By comparing its fluorescence emission with the control buffer and with the non-fluorescent T22-HSNBT-H6 (Supplementary Fig. 3C), we observed clear and functional fluorescence emission, thus confirming that a proper folding was retained by released protein species.

The asymptotic protein released from most of the generated depots

suggested the occurrence of a certain fraction of protein not releasable by mere incubation in physiological buffer (Fig. 2A, C). However, when the depots incubated in buffer and exhausted for 21 days were further exposed to EDTA, the chelation of metals released additional protein amounts (Fig. 2D) without the complete solubilization of the granules. In this regard, a certain fraction of the depot protein (ranging from <1 % to around 87 %) was still reluctant to chelation and therefore not available (Fig. 2D). Overall, the high variability in the amount of available protein indicated again that protein features determine the solubilization potential from the granules and confirmed the moderate impact of the cation formulation, used for fabrication, on the disintegration process.

The nature of the core protein reluctant to release, was however unclear. In previous studies we had demonstrated that soluble histidine (but not other amino acids), added to the media, disrupted the metal-assisted oligomerization of His-tagged proteins [30], being such nano-scale oligomers intermediates in the formation of micro-scale granules [31]. However, since Cys residues might be potentially involved in the clustering of polypeptides and partially responsible from the occurrence of recalcitrant cores, a select subset of granules precipitated with $ZnCl_2$ was submitted to a further solubilization with DTT and EDTA, to explore the potential fraction of thiol-bound protein (Supplementary Fig. 3D). The results indicated that 100, 26.7 or 15.6 % of the protein remaining in the recalcitrant cores of T22-GFP-H6, EPIXRK-GFP-H6 and T22-HSNBT-H6, respectively, could be further released under specific reduction and chelation conditions. For the last two proteins, that exhibited a recalcitrant core even after reduction and chelation, we conducted a comprehensive study of their amyloid content, previously detected and believed to contribute to the mechanical stability of the materials [7]. For T22-HSNBT-H6, we employed the ThT assay (Supplementary Fig. 3E), while for the intrinsically fluorescent EPIXRK-GFP-H6, we obtained the ATR-FTIR spectra (Supplementary Fig. 3F). Both analyses provided compelling evidence of the amyloid content in the granules, confirming previous determinations with similar His-tagged proteins [7].

Envisaging a clinical applicability of secretory granules based on spontaneous self-disintegration, identifying such key protein features might allow discarding specific protein drugs from their administration in such a format, since low release/availability values would not result in a biologically relevant impact, as desired in a drug. For that, biochemical parameters and protein leakage data were compared pairwise (Fig. 3A, Supplementary Table 3). In this context, protein release average (R_{AVG}, Fig. 2B) and protein availability (upon forced, chelation-assisted release, Fig. 2D) correlated well (Fig. 3B, $r = 0.7$, $p = 0.0074$). This fact indicated that the EDTA-assisted protein solubilization from depots and the spontaneous protein release when these granules were in buffer were not different events, but temporal pieces of the same category of disintegration event. Therefore, this observation also confirmed that the protein release in buffer was based on the spontaneous chelation of the gluing cations, which having a biochemical limit in a buffered closed solution might be further exploited by the addition in EDTA.

In the whole comparison and among the other tested parameters, the instability index was found as inversely determinant of both protein release (Fig. 3C, $r = -0.7$, $p = 0.0061$) and availability (Fig. 3D, $r = -0.9$, $p < 0.0001$), while in the case of the GRAVY (Grand average of hydropathy) index, protein release correlated in the border of

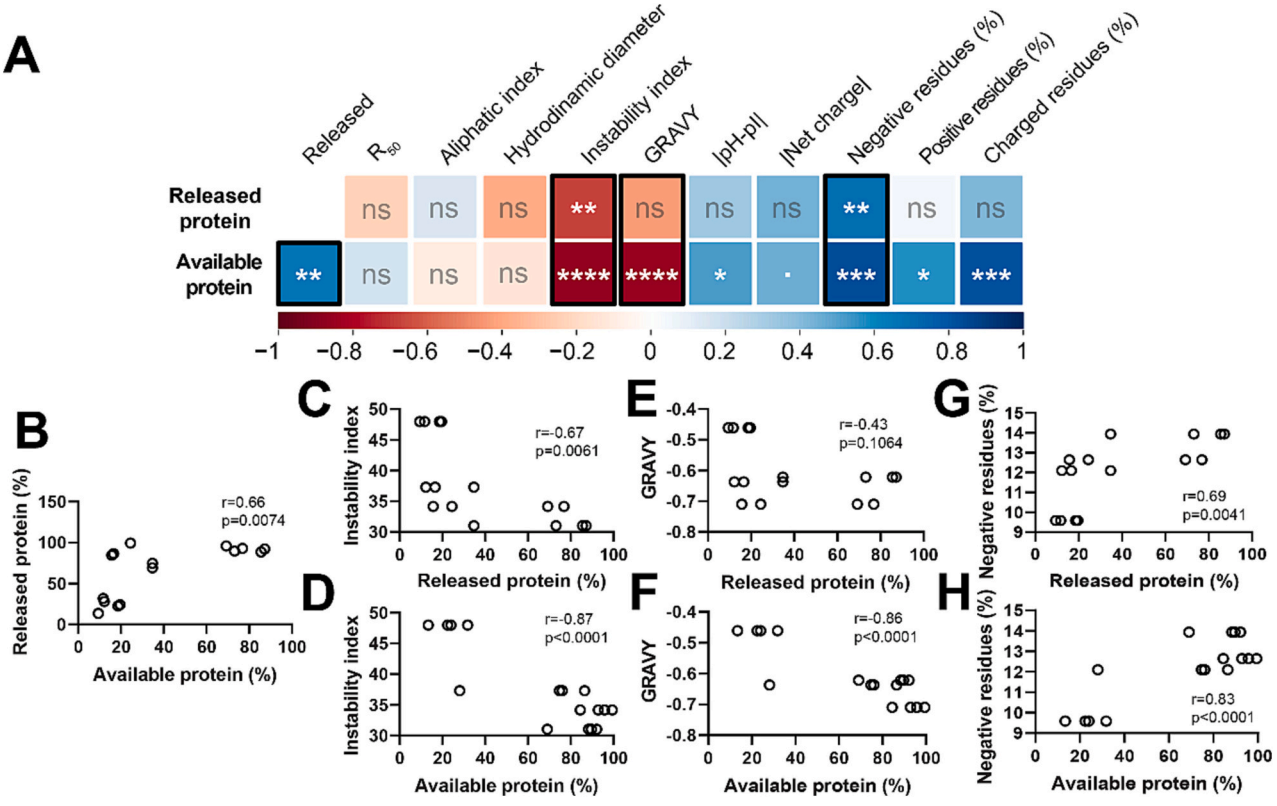

Fig. 3. A. Correlation matrix of relevant physicochemical parameters against the average released protein (R_{AVG}, Fig. 2B) or available protein (Fig. 2D), regardless of the divalent cation used for granule precipitation. A red-white-blue color gradient is used to represent Pearson r correlation scores from −1 to 1. Higher color saturation indicates a stronger negative (red) or positive (blue) correlation. Statistical significance is represented as · ($p < 0.1$), * ($p < 0.05$), ** ($p < 0.01$), *** ($p < 0.001$), **** ($p < 0.0001$) and ns (not significant). Pairwise correlations further explored in panels B to H are highlighted with a black border. B. Pairwise comparison displaying the relationship between released protein and available protein levels. C, D. Pairwise comparison demonstrating the correlation between the instability index and protein releasability or availability, respectively. E, F. Pairwise comparison featuring the association between the GRAVY index and protein releasability or availability, respectively. G, H. Pairwise comparison showcasing the relationship between the proportion of negative residues and protein releasability or availability, respectively.

significance (Fig. 3E, $r = -0.4$, $p = 0.1064$) but fully consistent with availability (Fig. 3F, $r = -0.9$, $p < 0.0001$). The dispersion of the isoelectric point regarding the pH of the release buffer and the absolute net charge of the protein (either positive or negative) were also slightly linked in a positive tendency to the amount of available protein ($r = 0.5$, $p = 0.0364$ and $p = 0.0713$, respectively). Lastly, the proportion of charged residues, and especially the ones with negative charge, was strongly and positively correlated with both the released (Fig. 3G, $r = 0.7$, $p = 0.0041$) and the available protein (Fig. 3H, $r = 0.8$, $p < 0.0001$). As seen in this case, but also applicable to the whole dataset, trends hinted by correlation data from released proteins are consolidated when the equivalent comparison is made using the available protein values. This is to be expected, as the statistical strength of the released protein variable relies on values of an arbitrary timespan (21 days), which is fairly representative but does not comprehend the entire nature of the material. This is in contraposition to the available protein variable, forced by EDTA chelation, that ultimately mirrors the release at a potentially indefinite amount of time.

4. Discussion

Secretory granules from the mammalian endocrine system store protein and peptidic hormones as amyloidal clusters, that belong to the so-called category of non-toxic, functional amyloids [10,11,32–34]. Zn, in its cationic form, sustains the amyloidal structure of these granules through coordination with the imidazole ring of histidine residues from different polypeptide chains, which result cross-linked [11,32]. Bacterial inclusion bodies show a similar amyloid architecture [35], in which histidine residues in the recombinant protein favor their clustering as insoluble aggregates in the bacterial cytoplasm [19]. Since an important fraction of the polypeptides embedded into inclusion bodies show a native or quasi-native conformation [36], they are releasable in vitro by mild solubilization treatments [37]. Because of the occurrence of such quasi-soluble fraction of active and functional protein in inclusion bodies, these microscale particles have been used in vivo, upon subcutaneous injection, as depots for prolonged protein drug delivery [38]. In the release of proteins from both secretory granules and bacterial inclusion bodies, chaperones from the media or intimately linked to the material are probably involved [32,39,40].

Recently, artificial versions of such amyloidal depots have been generated by very simple fabrication protocols, consisting in the gentle mixing of his-tagged pure proteins with divalent cations [9,21]. Importantly, most of recombinant proteins produced by recombinant DNA technologies are his-tagged [41], what allows widely exploiting the clustering properties of Zn and other divalent cations that are usually present in the healthy mammalian body (and therefore, biocompatible [42]). In this regard, the concentration of metals used for the fabrication process (10 mM for Zn) is higher than the local levels found in the human body (2–15 μM for Zn, [43]), thus preventing an in vivo reversion of the disintegration process. However, they are far below the recommended daily uptake [44], making the materials safe in this regard. The resulting microscale granules show slow release (for weeks) of the forming protein upon subcutaneous administration in vivo and also in vitro, at 37 °C and at physiological pH [4,27]. This is probably occurring by the natural dilution of the gluing metal in the body tissues or/and by the action of the abounding natural chelators [45,46]. The released protein is mostly found in a nanoscale oligomeric form, and when containing GFP, fully fluorescent (Supplementary Fig. 3). This is indicative of a proper folding status of the leaked protein, what is in agreement by previous studies in which released targeted peptides [7], cytotoxic proteins [7,8] or growth factors or enzymes [47] performed their expected functionalities upon release.

In contrast with bacterial inclusion bodies, which are heterogeneous mixtures of the recombinant protein plus bacterial molecules (proteins, nucleic acids, and cell wall components, [48,49]), the synthetic versions are chemically pure and can smoothly face a clinical development. A main concern about the design and use of such dynamic depots is how the disintegration process does occur, and how it can be modulated for a higher performance of the drug delivery platform. Obviously, in contrast to secretory granules for hormone storage and release, or to inclusion bodies (intracellular protein repositories), intrinsic chaperone activities can be discarded as promoters of disintegration. Here we have demonstrated that the cation used for clustering has only a moderate influence on the amount of protein that can be spontaneously released in buffer or removed by EDTA addition (Fig. 2A–D), even ion Ca is clearly less efficient that other tested formulations in the aggregation process (Fig. 1C). This fact indicates that the position of the cation in the Irving-Williams series [50] and the resulting strength of the coordination are not straightforwardly responsible for favored protein release or retention. On the other hand, different proteins (Fig. 1A) with distinguishable biochemical properties (Fig. 1B) show divergent patterns of protein release (Fig. 2A–C). When screening such properties, instability and hydropathicity indexes show an inverse correlation with the soluble protein fraction upon both spontaneous disintegration in buffer or EDTA-assisted disassembling of the material (Fig. 3C–F). The instability index estimates a protein's stability in a test tube, based on previous studies that identified specific dipeptides showing significant differences in occurrence between unstable and stable proteins [51]. To each of the 400 different dipeptides studied was assigned a weight value of instability, allowing the computation of an instability index. A value below 40 predicts protein stability, while a value above 40 suggests potential instability. Among the four tested proteins in our study, T22-HSNBT-H6 is the only one with an instability index above 40 (47.99) and, interestingly, the one that exhibited the higher proportion of insoluble protein remaining in the granule at the end of the incubation assay. This case serves as a prominent example that underpins the observed the correlation (Fig. 3C, D) between higher instability and an increased propensity for protein insolubility, thus reinforcing its significance.

The proportion of negatively charged residues also shows an impact (Fig. 3G, H). In fact, GFP-H6, that in contrast to the other three model proteins lacks a positive net charge at the amino terminus, (Fig. 1A) is more reluctant to aggregation (Fig. 1C) and the aggregates are more rapidly disintegrated in vitro than those formed by other proteins (Fig. 2A, B). The total fraction of available protein is higher in the aggregates formed by this protein version (Fig. 2C, D). In fact, cationic peptides at the amino terminus have previously been demonstrated to position monomers for the formation of nanoscale protein oligomers [52], which in this case are driven by the coordinating H6 tag. Then, the occurrence of a cationic peptide at the protein amino terminus is an enhancer of both aggregation and prolonged time-release of protein from the formed aggregates. Such type of peptides might also favor the release of protein in form of relatively stable nanoscale oligomers [53] as seen here (Sup. Fig. 3B), that for applications in nanomedicine is highly interesting since this fact would provide a multiple presentation of cell-targeting agents or functional protein drugs [54–56].

Importantly, the amount of released protein (in buffer) correlates well with the amount of available protein (Fig. 3B), understanding such protein fraction as the total amount that can be extracted from the aggregates by EDTA addition. A certain fraction of protein, a granule core reluctant to solubilization, variable when comparing proteins (Fig. 3D), might correspond to amyloidal protein, that at least in some specific polypeptides has been estimated to be around 40 % in both bacterial inclusion bodies and in synthetic secretory granules. Such good correlation between released and available protein as stressed above (Fig. 3B), indicates that the spontaneous disintegration of granules observed in vitro and in vivo [4,27] that allows the release of functional protein is caused by the progressive chelation of the clustering ion without any potential additional mechanism. The rate and profile in which this event occurs, is mediated, as supported by the present data, by precise biochemical properties of the protein building block.

5. Conclusion

Synthetic protein microscale granules, fabricated through the controlled coordination between divalent cations and His residues, are convenient time sustained delivery systems for protein drugs, which mimic secretory amyloids from the endocrine system and other natural protein depots, such as bacterial inclusion bodies in recombinant bacteria. The particular divalent cation used for clustering of His-tagged proteins into such dynamic depots has only a moderate impact on the availability of the protein and on the kinetics of its physiological release. However, key properties of the building block protein such as instability and hydropathicity, and at minor extent, its anionic character, dramatically influence the pattern of leakage and the amount of material that can be made available from a recalcitrant core. On the other hand, the spontaneous disintegration of the microgranules is a chelation-linked event, in which the gluing cation is progressively detached from the material. Knowing the protein properties that determine the disintegration rate and the extent of biological availability is essential for the design of advanced drug delivery systems with secretory properties. Being mechanically stable and resulting from easy fabrication processes, synthetic secretory depots emerge as extremely useful tools in the biomedicine of conditions that require a sustained supply of functional proteins. In addition, these microscale depots are based in self-organizing principles in which the building block protein act as both the drug and the scaffold that provides mechanical stability to the material. This fact allows skipping the use of chemically heterogeneous holding porous materials or matrices, which might pose biocompatibility and toxicity issues when designing a specific controlled drug release platform.

CRediT authorship contribution statement

Eloi Parladé: Methodology, investigation, formal analysis, visualization and manuscript writing, review and editing.

Hèctor-López-Laguna: Methodology, investigation, and manuscript review.

Julieta M. Sánchez and Ugutz Unzueta: Methodology, manuscript review and editing.

Antonio Villaverde and Esther Vázquez: Conceptualization, supervision, funding acquisition and manuscript writing, review and editing.

Declaration of competing interest

JMS, HLL, AV and EV are coauthors of a patent covering the use of artificial secretory granules. The other authors declare no conflict of interest.

Data availability

Data can be retrieved from the following site: doi:10.34810/data613.

Acknowledgements

The authors appreciate the financial support received for the development of multimeric recombinant drugs, from AEI (PID2019-105416RB-I00/AEI/10.13039/501100011033 and PDC2022-133858I00/AEI/10.13039/501100011033/Unión Europea NextGenerationEU/PRTR to E.V. and PID2020-116174RB-I00 to A.V.), AGAUR (2020PANDE00003 and 2021SGR00092 to A.V.), Instituto de Salud Carlos III (PI20/00400 to U.U.) co-funded by European Regional Development Fund (ERDF, a way to make Europe). JMS is supported with a María Zambrano postdoctoral researcher contract (677904) from Ministerio de Universidades and European Union ("Financed by European Union-Next GenerationEU"). U.U. is supported by Miguel Servet contract (CP19/00028) from ISCIII co-funded by European Social Fund (ESF investing in your future). We also appreciate the funding from the CIBER -Consorcio Centro de Investigación Biomédica en Red- (CB06/01/0014), Instituto de Salud Carlos III, Ministerio de Ciencia e Innovación, through several projects (VENOM4CANCER to A.V., NANOREMOTE to E.V. and NANOSCAPE to U.U). A.V. received an ICREA ACADEMIA award. Protein production was partially performed by the ICTS "NANBIOSIS", more specifically by the Protein Production Platform of CIBER in Bioengineering, Biomaterials & Nanomedicine (CIBER-BBN)/IBB, at the UAB (http://www.nanbiosis.es/portfolio/u1-protein-production-platform-ppp/).

Appendix A. Supplementary data

Supplementary data to this article can be found online at https://doi.org/10.1016/j.ijbiomac.2023.126164.

References

[1] J. Li, D.J. Mooney, Designing hydrogels for controlled drug delivery, Nat. Rev. Mater. 1 (2016), https://doi.org/10.1038/natrevmats.2016.71.
[2] W.B. Liechty, D.R. Kryscio, B.V. Slaughter, N.A. Peppas, Polymers for drug delivery systems, Annu. Rev. Chem. Biomol. Eng. 1 (2010), https://doi.org/10.1146/annurev-chembioeng-073009-100847.
[3] W. Huang, P. Hao, J. Qin, S. Luo, T. Zhang, B. Peng, H. Chen, X. Zan, Hexahistidine-metal assemblies: a promising drug delivery system, Acta Biomater. 90 (2019), https://doi.org/10.1016/j.actbio.2019.03.058.
[4] L. Zhao, L. Luo, F. Meng, Metal-mediated nanobody assemblies as potent alleviators of human islet amyloid polypeptide aggregation, Mater. Chem. Front. 7 (10) (2023), https://doi.org/10.1039/D2QM01372J.
[5] M. Yang, W.J. Song, Diverse protein assembly driven by metal and chelating amino acids with selectivity and tunability, Nat. Commun. 10 (2019), https://doi.org/10.1038/s41467-019-13491-w.
[6] O. Cano-Garrido, N. Serna, U. Unzueta, E. Parladé, R. Mangues, A. Villaverde, E. Vázquez, Protein scaffolds in human clinics, Biotechnol. Adv. 61 (2022), 108032, https://doi.org/10.1016/J.BIOTECHADV.2022.108032.
[7] J.M. Sánchez, H. López-Laguna, P. Álamo, N. Serna, A. Sánchez-Chardi, V. Nolan, O. Cano-Garrido, I. Casanova, U. Unzueta, E. Vazquez, R. Mangues, A. Villaverde, Artificial inclusion bodies for clinical development, Adv. Sci. 7 (2020), https://doi.org/10.1002/advs.201902420.
[8] N. Serna, O. Cano-Garrido, J.M. Sánchez, A. Sánchez-Chardi, L. Sánchez-García, H. López-Laguna, E. Fernández, E. Vázquez, A. Villaverde, Release of functional fibroblast growth factor-2 from artificial inclusion bodies, J. Control Release (2020), https://doi.org/10.1016/j.jconrel.2020.08.007.
[9] T.Y. Chen, W.J. Cheng, J.C. Horng, H.Y. Hsu, Artificial peptide-controlled protein release of Zn2+-triggered, self-assembled histidine-tagged protein microparticle, Colloids Surf. B: Biointerfaces 187 (2020), https://doi.org/10.1016/j.colsurfb.2019.110644.
[10] R.S. Jacob, S. Das, S. Ghosh, A. Anoop, N.N. Jha, T. Khan, P. Singru, A. Kumar, S. K. Maji, Amyloid formation of growth hormone in presence of zinc: Relevance to its storage in secretory granules, Sci. Rep. (2016), https://doi.org/10.1038/srep23370.
[11] R.S. Jacob, S. Das, S. Ghosh, A. Anoop, N.N. Jha, T. Khan, P. Singru, A. Kumar, S. K. Maji, Amyloid formation of growth hormone in presence of zinc: relevance to its storage in secretory granules, Sci. Rep. 6 (2016) 1–18, https://doi.org/10.1038/srep23370.
[12] S.A. Levkovich, E. Gazit, D. Laor Bar-Yosef, Two decades of studying functional amyloids in microorganisms, Trends Microbiol. 29 (2021), https://doi.org/10.1016/j.tim.2020.09.005.
[13] A.V. Sergeeva, A.P. Galkin, Functional amyloids of eukaryotes: criteria, classification, and biological significance, Curr. Genet. 66 (2020), https://doi.org/10.1007/s00294-020-01079-7.
[14] A. Balistreri, E. Goetzler, M. Chapman, Functional amyloids are the rule rather than the exception in cellular biology, Microorganisms. 8 (2020), https://doi.org/10.3390/microorganisms8121951.
[15] A. Soragni, S.K. Maji, R. Riek, Toward a comprehension of functional aggregation into amyloids in pituitary secretory granules, Amyloid 17 (2010).
[16] S.K. Maji, M.H. Perrin, M.R. Sawaya, S. Jessberger, K. Vadodaria, R.A. Rissman, P. S. Singru, K.P.R. Nilsson, R. Simon, D. Schubert, D. Eisenberg, J. Rivier, P. Sawchenko, W. Vale, R. Riek, Functional amyloids as natural storage of peptide hormones in pituitary secretory granules, Science 325 (2009) (1979) 328–332, https://doi.org/10.1126/SCIENCE.1173155/SUPPL_FILE/MAJI.SOM.PDF.
[17] L.C.S. Erthal, A.F. Marques, F.C.L. Almeida, G.L.M. Melo, C.M. Carvalho, L. C. Palmieri, K.M.S. Cabral, G.N. Fontes, L.M.T.R. Lima, Regulation of the assembly and amyloid aggregation of murine amylin by zinc, Biophys. Chem. 218 (2016), https://doi.org/10.1016/j.bpc.2016.09.008.
[18] Y. Jiang, K. Shi, D. Xia, H. Piao, P. Quan, T. Song, F. Cui, Protamine modified metal ion-protein chelate microparticles for sustained release of interferon, Int. J. Pharm. 407 (2011), https://doi.org/10.1016/j.ijpharm.2011.01.003.
[19] J.M. Sánchez, J.V. Carratalá, N. Serna, U. Unzueta, V. Nolan, A. Sánchez-Chardi, E. Voltà-Durán, H. López-Laguna, N. Ferrer-Miralles, A. Villaverde, E. Vazquez, The poly-histidine tag H6 mediates structural and functional properties of

disintegrating, protein-releasing inclusion bodies, Pharmaceutics 14 (2022) 602, https://doi.org/10.3390/PHARMACEUTICS14030602.
[20] J. Shen, J. Wolfram, M. Ferrari, H. Shen, Taking the vehicle out of drug delivery, Mater. Today 20 (2017), https://doi.org/10.1016/j.mattod.2017.01.013.
[21] H. López-Laguna, E. Parladé, P. Álamo, J.M. Sánchez, E. Voltà-Durán, N. Serna, L. Sánchez-García, O. Cano-Garrido, A. Sánchez-Chardi, A. Villaverde, R. Mangues, U. Unzueta, E. Vázquez, H. López-Laguna, E. Parladé, J.M. Sánchez, E. Voltà-Durán, N. Serna, L. Sánchez-García, A. Villaverde, E. Vázquez, P. Álamo, U. Unzueta, R. Mangues, In Vitro Fabrication of Microscale Secretory Granules, 2021, https://doi.org/10.1002/adfm.202100914.
[22] C. Debdeep, S.J. Reeba, R. Soumik, N. Ambuja, S. Namrata, S. Shinjinee, G. Laxmikant, K. Pradeep, D. Debalina, P. Ajoy, A. Sakunthala, M. Surabhi, P. Chinmai, K. Santosh, S. Praful, S. Sanjib, K.M. Samir, Co-aggregation and secondary nucleation in the life cycle of human prolactin/galanin functional amyloids, eLife 11 (2022), https://doi.org/10.7554/eLife.73835.
[23] J.L. Corchero, M.T.P. Favaro, M. Márquez-Martínez, J. Lascorz, C. Martínez-Torró, J.M. Sánchez, H. López-Laguna, L.C. de Souza Ferreira, E. Vázquez, N. Ferrer-Miralles, A. Villaverde, E. Parladé, Recombinant proteins for assembling as nano- and micro-scale materials for drug delivery: A host comparative overview, Pharmaceutics (2023), https://doi.org/10.3390/pharmaceutics15041197.
[24] N. Serna, A. Falgàs, A. García-León, U. Unzueta, Y. Núñez, A. Sánchez-Chardi, C. Martínez-Torró, R. Mangues, E. Vazquez, I. Casanova, A. Villaverde, Time-prolonged release of tumor-targeted protein–MMAE nanoconjugates from implantable hybrid materials, Pharmaceutics. 14 (2022), https://doi.org/10.3390/pharmaceutics14010192.
[25] O. Cano-Garrido, P. Álamo, L. Sánchez-García, A. Falgàs, A. Sánchez-Chardi, N. Serna, E. Parladé, U. Unzueta, M. Roldán, E. Voltà-Durán, I. Casanova, A. Villaverde, R. Mangues, E. Vázquez, Biparatopic protein nanoparticles for the precision therapy of cxcr4+ cancers, Cancers 13 (2021), https://doi.org/10.3390/cancers13122929.
[26] P. Álamo, J. Cedano, O. Conchillo-Sole, O. Cano-Garrido, L. Alba-Castellon, N. Serna, A. Aviñó, L.M. Carrasco-Diaz, A. Sánchez-Chardi, C. Martinez-Torró, A. Gallardo, M. Cano, R. Eritja, A. Villaverde, R. Mangues, E. Vazquez, U. Unzueta, Rational engineering of a human GFP-like protein scaffold for humanized targeted nanomedicines, Acta Biomater. 130 (2021), https://doi.org/10.1016/j.actbio.2021.06.001.
[27] P. Álamo, E. Parladé, H. López-Laguna, E. Voltà-Durán, U. Unzueta, E. Vazquez, R. Mangues, A. Villaverde, Ion-dependent slow protein release from in vivo disintegrating micro-granules 28, 2021, pp. 2383–2391, https://doi.org/10.1080/10717544.2021.1998249.
[28] M.R. Wilkins, E. Gasteiger, A. Bairoch, J.C. Sanchez, K.L. Williams, R.D. Appel, D. F. Hochstrasse, Protein identification and analysis tools in the ExPASy server, Methods Mol. Biol. 112 (1999) 531–552, https://doi.org/10.1385/1-59259-584-7.
[29] D. Osorio, P. Rondón-Villarreal, R. Torres, Peptides: a package for data mining of antimicrobial peptides, R J. 7 (2015), https://doi.org/10.32614/rj-2015-001.
[30] H. López-Laguna, U. Unzueta, O. Conchillo-Solé, A. Sánchez-Chardi, M. Pesarrodona, O. Cano-Garrido, E. Voltà, L. Sánchez-García, N. Serna, P. Saccardo, R. Mangues, A. Villaverde, E. Vázquez, Assembly of histidine-rich protein materials controlled through divalent cations, Acta Biomater. 83 (2019), https://doi.org/10.1016/j.actbio.2018.10.030.
[31] H. López-Laguna, J.M. Sánchez, J.V. Carratalá, M. Rojas-Peña, L. Sánchez-García, E. Parladé, A. Sánchez-Chardi, E. Voltà-Durán, N. Serna, O. Cano-Garrido, S. Flores, N. Ferrer-Miralles, V. Nolan, A. de Marco, N. Roher, U. Unzueta, E. Vazquez, A. Villaverde, Biofabrication of functional protein nanoparticles through simple His-tag engineering, ACS Sustain. Chem. Eng. 9 (2021), https://doi.org/10.1021/acssuschemeng.1c04256.
[32] R.S. Jacob, A. Anoop, S.K. Maji, Protein nanofibrils as storage forms of peptide drugs and hormones, Adv. Exp. Med. Biol. 1174 (2019) 265–290, https://doi.org/10.1007/978-981-13-9791-2_8/FIGURES/5.
[33] M. Spiess, N. Beuret, C. Prescianotto Baschong, J. Rutishauser, Amyloid-like aggregation of provasopressin, in: Vitam Horm, 2020, https://doi.org/10.1016/bs.vh.2019.08.014.
[34] B.M. Jayawardena, M.R. Jones, Y. Hong, C.E. Jones, Copper ions trigger disassembly of neurokinin B functional amyloid and inhibit de novo assembly, J. Struct. Biol. 208 (2019), https://doi.org/10.1016/j.jsb.2019.09.011.
[35] A. De Marco, N. Ferrer-Miralles, E. Garcia-Fruitós, A. Mitraki, S. Peternel, U. Rinas, M.A. Trujillo-Roldán, N.A. Valdez-Cruz, E. Vázquez, A. Villaverde, Bacterial inclusion bodies are industrially exploitable amyloids, FEMS Microbiol. Rev. 43 (2019), https://doi.org/10.1093/femsre/fuy038.
[36] N. Gonzalez-Montalban, E. Garcia-Fruitos, A. Villaverde, Recombinant protein solubility[mdash]does more mean better? Nat. Biotechnol. 25 (2007) 718–720, https://doi.org/10.1038/nbt0707-718.
[37] P. Singhvi, A. Saneja, S. Srichandan, A.K. Panda, Bacterial inclusion bodies: a treasure trove of bioactive proteins, Trends Biotechnol. 38 (2020), https://doi.org/10.1016/j.tibtech.2019.12.011.
[38] M.V. Céspedes, O. Cano-Garrido, P. Álamo, R. Sala, A. Gallardo, N. Serna, A. Falgàs, E. Voltà-Durán, I. Casanova, A. Sánchez-Chardi, H. López-Laguna, L. Sánchez-García, J.M. Sánchez, U. Unzueta, E. Vázquez, R. Mangues, A. Villaverde, Engineering secretory amyloids for remote and highly selective destruction of metastatic foci, Adv. Mater. 32 (2020), https://doi.org/10.1002/adma.201907348.
[39] M.M. Carrió, A. Villaverde, Localization of chaperones DnaK and GroEL in bacterial inclusion bodies, J. Bacteriol. 187 (2005) 3599–3601.
[40] J. Weibezahn, B. Bukau, A. Mogk, Unscrambling an egg: protein disaggregation by AAA+ proteins, Microb. Cell Factories 3 (2004), https://doi.org/10.1186/1475-2859-3-1.
[41] H. López-Laguna, E. Voltà-Durán, E. Parladé, A. Villaverde, E. Vázquez, U. Unzueta, Insights on the emerging biotechnology of histidine-rich peptides, Biotechnol. Adv. 54 (2022), 107817, https://doi.org/10.1016/J.BIOTECHADV.2021.107817.
[42] H. López-Laguna, J. Sánchez, U. Unzueta, R. Mangues, E. Vázquez, A. Villaverde, Divalent cations: a molecular glue for protein materials, Trends Biochem. Sci. 45 (2020) 992–1003, https://doi.org/10.1016/J.TIBS.2020.08.003.
[43] K.L. Chang, T.C. Hung, B.S. Hsieh, Y.H. Chen, T.F. Chen, H.L. Cheng, Zinc at pharmacologic concentrations affects cytokine expression and induces apoptosis of human peripheral blood mononuclear cells, Nutrition. 22 (2006), https://doi.org/10.1016/j.nut.2005.11.009.
[44] H. López-Laguna, J. Sánchez, U. Unzueta, R. Mangues, E. Vázquez, A. Villaverde, Divalent cations: a molecular glue for protein materials trends in biochemical sciences an official publication of the International Union of Biochemistry and Molecular Biology, Trends Biochem. Sci. 45 (2020), https://doi.org/10.1016/j.tibs.2020.08.003.
[45] G.J. Kontoghiorghes, A. Kolnagou, Molecular factors and mechanisms affecting iron and other metal excretion or absorption in health and disease. The role of natural and synthetic chelators, Curr. Med. Chem. 12 (2005), https://doi.org/10.2174/092986705774463030.
[46] W. Jung, D.Y. Lee, E. Moon, S. Jon, Nanoparticles derived from naturally occurring metal chelators for theranostic applications, Adv. Drug Deliv. Rev. 191 (2022), https://doi.org/10.1016/j.addr.2022.114620.
[47] J.M. Sanchez, H. López-Laguna, N. Serna, U. Unzueta, P.D. Clop, A. Villaverde, E. Vazquez, Engineering the performance of artificial inclusion bodies built of catalytic β-galactosidase, ACS Sustain. Chem. Eng. 9 (2021), https://doi.org/10.1021/acssuschemeng.0c08345.
[48] P. Valax, G. Georgiou, Molecular characterization of β-lactamase inclusion bodies produced in Escherichia coli. 1. Composition, Biotechnol. Prog. 9 (1993), https://doi.org/10.1021/bp00023a014.
[49] E. Krachmarova, I. Ivanov, G. Nacheva, Nucleic acids in inclusion bodies obtained from E. coli cells expressing human interferon-gamma, Microb. Cell Factories 19 (2020), https://doi.org/10.1186/s12934-020-01400-6.
[50] D.A. Johnson, P.G. Nelson, Factors determining the ligand field stabilization energies of the hexaaqua 2+ complexes of the first transition series and the Irving-Williams order, Inorg. Chem. 34 (1995), https://doi.org/10.1021/ic00126a041.
[51] K. Guruprasad, B.V.B. Reddy, M.W. Pandit, Correlation between stability of a protein and its dipeptide composition: a novel approach for predicting in vivo stability of a protein from its primary sequence, Protein Eng. Des. Sel. 4 (1990), https://doi.org/10.1093/protein/4.2.155.
[52] U. Unzueta, N. Ferrer-Miralles, J. Cedano, X. Zikung, M. Pesarrodona, P. Saccardo, E. García-Fruitós, J. Domingo-Espín, P. Kumar, K.C. Gupta, R. Mangues, A. Villaverde, E. Vazquez, Non-amyloidogenic peptide tags for the regulatable self-assembling of protein-only nanoparticles, Biomaterials. 33 (2012), https://doi.org/10.1016/j.biomaterials.2012.08.033.
[53] F. Rueda, M.V. Céspedes, O. Conchillo-Solé, A. Sánchez-Chardi, J. Seras-Franzoso, R. Cubarsi, A. Gallardo, M. Pesarrodona, N. Ferrer-Miralles, X. Daura, E. Vázquez, E. García-Fruitós, R. Mangues, U. Unzueta, A. Villaverde, Bottom-up instructive quality control in the biofabrication of smart protein materials, Adv. Mater. (2015), https://doi.org/10.1002/adma.201503676.
[54] U. Unzueta, M.V. Céspedes, E. Vázquez, N. Ferrer-Miralles, R. Mangues, A. Villaverde, Towards protein-based viral mimetics for cancer therapies, Trends Biotechnol. 33 (2015), https://doi.org/10.1016/j.tibtech.2015.02.007.
[55] R. Sala, L. Sánchez-García, N. Serna, M.V. Céspedes, I. Casanova, M. Roldán, A. Sánchez-Chardi, U. Unzueta, E. Vázquez, R. Mangues, A. Villaverde, Collaborative membrane activity and receptor-dependent tumor cell targeting for precise nanoparticle delivery in $CXCR4^{+}$ colorectal cancer, Acta Biomater. 99 (2019), https://doi.org/10.1016/j.actbio.2019.09.002.
[56] M.V. Céspedes, U. Unzueta, W. Tatkiewicz, A. Sánchez-Chardi, O. Conchillo-Solé, P. Álamo, Z. Xu, I. Casanova, J.L. Corchero, M. Pesarrodona, J. Cedano, X. Daura, I. Ratera, J. Veciana, N. Ferrer-Miralles, E. Vazquez, A. Villaverde, R. Mangues, In vivo architectonic stability of fully de novo designed protein-only nanoparticles, ACS Nano 8 (2014), https://doi.org/10.1021/nn4055732.